Spatial Resolution Enhancement of Coherent Doppler Lidar by Pseudo-Random Phase Coding

Yunpeng Zhang, Yunbin Wu, and Haiyun Xia

***Abstract*—A high spatial resolution coherent Doppler wind lidar (CDWL) incorporating pseudo-random phase coding (PRPC) is proposed and demonstrated. Random phase coding of the transmitted lightwave spreads the atmospheric backscattered spectrum and the spatial resolution can be enhanced as only the signal with specific time delay could be despread during decoding. The narrow peak of the despread spectrum provides higher wind velocity retrieval accuracy compared with conventional pulsed CDWL with the same spatial resolution. Spectrum difference is applied to reduce the interference between the spread and despread spectra. The new method's performance is verified in a comparison experiment with a non-coding CDWL. Continuous radial wind profile measurement over 800 m is demonstrated with spatial/temporal resolution of 4.5 m/1 s, at laser peak power of 250 W.**

***Index Terms*—Coherent doppler lidar, phase modulation, pseudo-random code, spatial resolution.**

I. Introduction

Doppler wind lidar is an active remote sensing technology that retrieves the wind velocity from atmospheric backscattered signal's Doppler frequency shift. Due to its inherent properties like high spatial/temporal resolution, Doppler wind lidar has been widely employed in scientific research and engineering applications, such as gravity waves monitoring [1], [2], boundary layer detection [3], wind energy exploitation [4], weather forecast [5], and air pollution analysis [6], [7]. With the help of heterodyne detection, a coherent Doppler wind lidar (CDWL) inherits the capability of retrieving not only the amplitude but also the phase of the atmospheric backscattered signal, supporting spectrum analysis based applications such as precipitation observation and cloud phase identification [8]–[10]. In applications like aviation safety and aerodynamic design, higher spatial resolution is required to realize fine measurement of the dynamic structure of aircraft wake vortex and turbulence [11]–[13]. However, it remains challenging to improve the spatial resolution of CDWLs to meter scale.

In conventional pulsed CDWL systems, the classical time-of-flight (TOF) method is employed to get the range resolved wind profile, where the spatial resolution depends on the pulse duration. Simply shortening the pulse duration will result in the broadening of backscattered spectra, thereby reducing the estimation accuracy of Doppler frequency shift [14], [15]. In addition, since the peak power of a laser amplifier is usually limited, the decrease of pulse duration will reduce the power of the atmospheric backscattered signal. Recently, several methods have been proposed to mitigate these negative effects. High peak power fiber laser [16] and high repetition rate coded pulse sequence [17] are used to compensate for the reduction of backscattered power related to the short pulse duration, but the broadened spectrum will still hinder the further improvement of spatial resolution. One attempt to avoid the spectrum broadening is the differential correlation pair (DCP) technique [18]. However, the realization of high spatial resolution with this technique requires precision waveform control of the pulse pair, which makes it vulnerable to environmental disturbance.

Phase coded modulation has been widely used in fields like microwave radar [19], ultrasonic ranging [20] and target-detection lidar [21]–[23] to enhance the system performance in aspects such as spatial resolution and Doppler tolerance. When applied in wind detection, the random distributed scattering feature of the atmospheric aerosols needs to be particularly addressed. Inspired by the direct sequence spread spectrum (DSSS) technology in digital communication [24], we turn to the spread-spectrum characteristic of the pseudo-random code to avoid distance aliasing caused by the distributed scattering.

In this work, we propose and demonstrate a new approach combining TOF and pseudo-random phase coding (PRPC) to enhance the spatial resolution of CDWLs. In the proposed scheme, the spatial resolution is determined by the modulation rate, while the width of the spectral main peak depends on the pulse duration. Thus, the constraint between the two parameters is relaxed, offering a new degree of freedom. Due to the spread-spectrum characteristic of the pseudo-random code, the interference of backscattered signals from different distances can be effectively reduced by the difference between spectrum before and after decoding. In a proof-of-concept experiment, the proposed scheme is compared with a conventional non-coding scheme,

Manuscript received January 3, 2022; revised February 26, 2022; accepted March 14, 2022. Date of publication March 17, 2022; date of current version July 2, 2022. This work was supported in part by National Ten Thousand Talent Program in China and in part by the Strategic Priority Research Program of Chinese Academy of Sciences under Grant XDA22040601. *(Corresponding author: Haiyun Xia.)*

Yunpeng Zhang and Yunbin Wu are with the School of Earth and Space Sciences, University of Science and Technology of China (USTC), Hefei 230026, China (e-mail: zyp110@mail.ustc.edu.cn; wuyunbin@mail.ustc.edu.cn).

Haiyun Xia is with the School of Earth and Space Sciences, University of Science and Technology of China (USTC), Hefei 230026, China, with the School of Atmospheric Physics, Nanjing University of Information Science and Technology, Nanjing 210044, China, with the Hefei National Laboratory for Physical Sciences at the Microscale, USTC, Hefei 230026, China, and also with the Institute of Software, Chinese Academy of Sciences, Beijing 100190, China (e-mail: hsia@ustc.edu.cn).

Color versions of one or more figures in this article are available at https://doi.org/10.1109/JLT.2022.3160294.

Digital Object Identifier 10.1109/JLT.2022.3160294

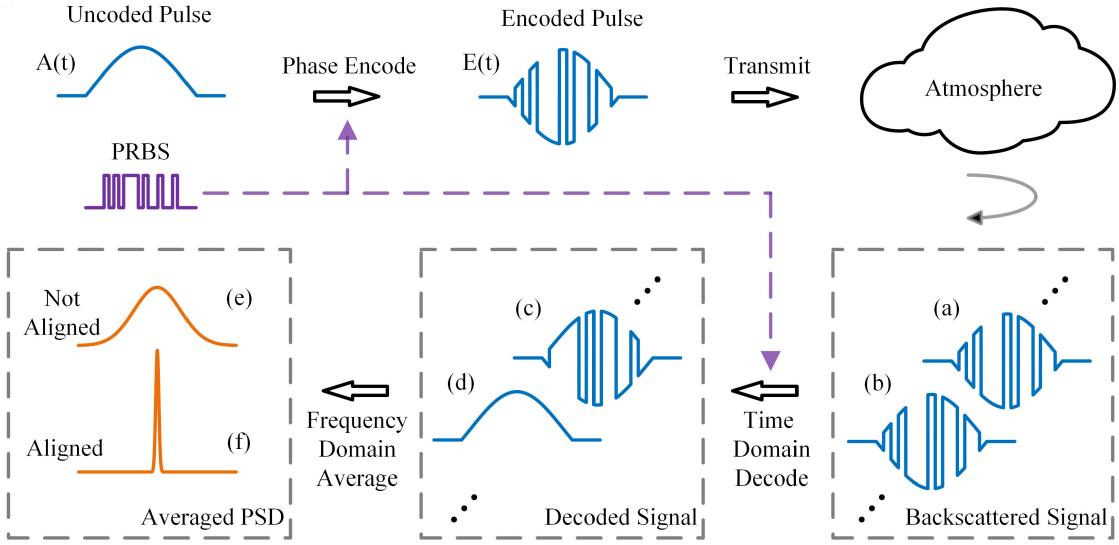

Fig. 1. Principle of the proposed pseudo-random phase coding lidar. Backscattered signal (a) not aligned (b) aligned to the decoding sequence; (c) Not aligned (d) aligned signal after decoding; Averaged Power spectral density (PSD) of the (e) not aligned (f) aligned signal.

thus validating its advantage of spatial resolution improvement without spectrum broadening. Furthermore, continuous radial wind profiling with the spatial and temporal resolution of 4.5 m and 1 s is realized. Since only minor hardware changes need to be made to the conventional pulsed CDWLs, the proposed scheme has the potential to significantly enhance the performance of existing systems.

II. Principle

A. CDWL With Pseudo-Random Phase Coding

The principle of the PRPC lidar is shown in Fig. 1. The transmitted pulse is phase encoded by a pseudo-random binary sequence (PRBS), and the electric field of the lightwave can be expressed as:

$$E(t) = A(t)\exp\left(j2\pi f_c t + j\theta(t)\right) \tag{1}$$

where $A(t)$ is the amplitude envelope of the uncoded pulse, f_c is the carrier frequency, and $\theta(t)$ is the coded phase. When the PRBS is mapped to 0 and π, the coded phase term can be simplified as:

$$B(t) = \exp\left(j\theta(t)\right) = \begin{cases} +1, & (\theta = 0) \\ -1, & (\theta = \pi) \end{cases} \tag{2}$$

According to the classical "feuilleté" model of atmospheric scattering [25], the transmitted pulse's backscattered signal can be modeled as the superposition of the random atmospheric reflections from different slices. After heterodyne detection, the received signal is:

$$r(t) = \int A\left(t - \frac{2z}{c}\right) B\left(t - \frac{2z}{c}\right)\kappa(z) \times \exp\left(j2\pi\left(f_c + f_d(z) - f_{LO}\right)t\right) dz \tag{3}$$

where $f_{LO} = f_c - f_{IF}$ is the frequency of the local oscillator with f_{IF} being the intermediate frequency (IF), $f_d(z)$ is the Doppler frequency shift caused by the motion of aerosols, and $\kappa(z)$ is a circular random variable representing the random scattering feature of the atmosphere. Constants are omitted from the equation for brevity.

To retrieve the wind velocity at distance z_0, the received signal $r(t)$ is truncated by a window function $W(t - t_0)$and then decoded with the delayed modulation sequence $B(t - t_0)$, where $t_0 = 2z_0/c$ is the TOF corresponding to z_0 and c is the speed of light. Substituting (1) and (2), the decoded signal is expressed as:

$$r_{de}(t) = \int B\left(t - \tfrac{2z}{c}\right) B\left(t - \tfrac{2z_0}{c}\right) A\left(t - \tfrac{2z}{c}\right) W\left(t - \tfrac{2z_0}{c}\right) \times \kappa(z)\exp\left(j2\pi\left(f_d(z) + f_{IF}\right)t\right) dz \tag{4}$$

As illustrated in Fig. 1(a) to (d), only signal well aligned to the decoding sequence can be decoded effectively. As the bit interval of the modulation sequence is T_b, we define the spatial resolution as:

$$\Delta z = \frac{1}{2} c T_b \tag{5}$$

The integral in (4) can be divided into two parts, corresponding to the non-aligned ($|z - z_0| > \Delta z/2$) and aligned ($|z - z_0| \le \Delta z/2$) signals. The former's power spectral density (PSD) is spread by the pseudo-random modulation while the latter's PSD is despread in the decoding, as shown in Fig. 1(e) and (f). Therefore, the PSD of the decoded signal is mainly composed of two parts, and the despread narrow one corresponds to the backscattered spectrum from z_0 with a spatial resolution of Δz.

To further clarify the spatial resolution of the PRPC scheme, a numerical simulation based on (4) is conducted, where the IF is set to be zero for brevity. The pulse intensity envelope is set to be a truncated Gaussian function with full width at half maximum (FWHM) of 135 ns and a matched window function is used. With a modulation bit interval of 30 ns, the decoded spectrum and its composition are illustrated in Fig. 2(a). Besides

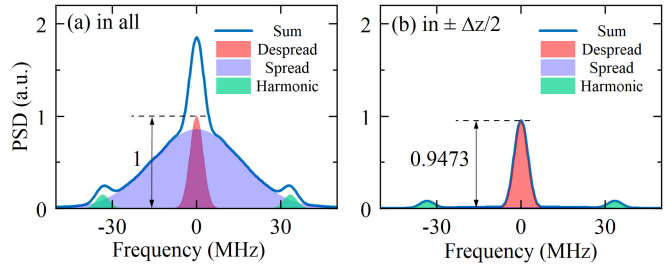

Fig. 2. Illustration of the spectral components in the decoded spectrum. (a) Signal from all scatters; (b) Signal from the scatters in a spatial resolution cell.

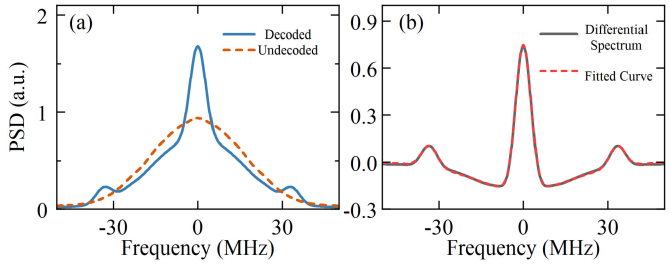

Fig. 3. (a) The decoded and undecoded spectrum; (b) The differential spectrum and its Gaussian fit.

the spread and despread parts, harmonic components centered at ±33.3 MHz can be observed, which are consistent with the modulation rate of $R_b = 1/T_b$. When limiting the integral region of (4) to $|z - z_0| \leq \Delta z/2$, the contribution of the backscattered signal in a spatial resolution cell can be extracted as in Fig. 2(b). Compared with Fig. 2(a), it can be seen that 95% of the despread component is contributed by the backscattered signal from an atmospheric cell within range Δz , which validates the definition of Δz as spatial resolution.

B. Spectrum Difference for Spatial Resolution Enhancement

Due to the overlap between the spectrum components, the frequency estimation of the despread part can be interfered by the spread part, which leads to the contamination of the spatial resolution. To overcome this obstacle, a spectrum difference technique is adopted.

Let Q_{sp} and Q_{ds} denote the spread and despread spectrum. As described above, the two portions in the decoded spectrum originate from the backscattered signal in and out of the spatial resolution cell, respectively. Thus, the decoded spectrum can be written as:

$$S_{de}(f; z_0) = Q_{ds}\left(f; |z - z_0| \leq \frac{\Delta z}{2}\right) + Q_{sp}\left(f; |z - z_0| > \frac{\Delta z}{2}\right) \quad (6)$$

On the other hand, if the received signal is not decoded, all the backscattered signal's spectrum would be spread, as illustrated in Fig. 3(a). Then, the undecoded spectrum is expressed as:

$$S_{un}(f; z_0) = Q_{sp}\left(f; |z - z_0| \leq \frac{\Delta z}{2}\right) + Q_{sp}\left(f; |z - z_0| > \frac{\Delta z}{2}\right) \quad (7)$$

The difference of the two spectra eliminates the signal outside the spatial resolution cell, resulting in:

$$\begin{aligned} S_D(f; z_0) &= S_{de}(f; z_0) - S_{un}(f; z_0) \\ &= Q_{ds}\left(f; |z - z_0| \leq \frac{\Delta z}{2}\right) \\ &\quad - Q_{sp}\left(f; |z - z_0| \leq \frac{\Delta z}{2}\right) \end{aligned} \quad (8)$$

The differential spectrum is shown in Fig. 3(b). Since the decoding does not change the signal's energy, the total area under the S_D curve should be zero, which leads to the negative part in the figure. As shown by the red dash line in Fig. 3(b), the differential spectrum can be well depicted by a 4-Gaussian model, where two of the functions are concentric and the other two have frequency shift of $\pm R_b$. The 4-Gaussian model can be used as a spectrum pattern to facilitate the center frequency estimation.

According to the presented analysis, the data processing algorithm of the PRPC lidar is summarized as Fig. 4.

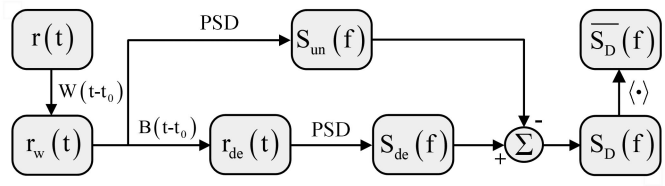

Fig. 4. Processing flow of the PRPC lidar algorithm, where $\langle\cdot\rangle$ refers to averaging over laser shots.

III. Experiment

A. System Layout

The system layout of the proposed PRPC lidar is shown in Fig. 5. A continuous-wave (CW) laser (Amonics ALiDAR-150-Seed) at 1550 nm is split into two parts, the major and minor portions serve as the seed of the transmitted pulse and the local oscillator (LO), respectively. The continuous seed is modulated into pulses with repetition rate of 12.5 kHz by an acousto-optic modulator (AOM). Meanwhile, a frequency shift of 80 MHz is introduced. The pulses are phase encoded by an electro-optic phase modulator (EOPM, iXblue MPZ-LN-20) with the half-wave voltage of 7 V. The PRBS is set to be a 10-bit M-sequence [24] prestored in an arbitrary wave generator (AWG, Keysight 33622A) with a length of 1000. The electrical signals feeding to the AOM and EOPM are triggered synchronously. And the time delay between the two driving signals is carefully adjusted by monitoring the modulated lightwave by homodyne detection, ensuring the alignment of the optical pulse

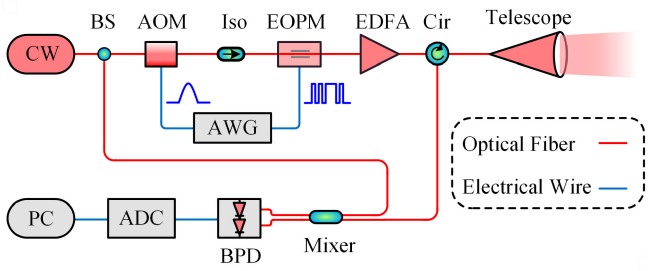

Fig. 5. System layout of the PRPC lidar. CW, continuous-wave laser; BS, beam splitter; Iso, isolator; AOM, acousto–optic modulator; EOPM, electro-optic phase modulator; EDFA, erbium-doped fiber amplifier; Cir, circulator; AWG, arbitrary wave generator; BPD, balanced photodetector; ADC, analog-to-digital converter; PC, personal computer.

TABLE I
SUMMARY OF KEY SYSTEM PARAMETERS

Parameters	Value
Transmitter:	
Center wavelength	1550.12 nm
Pulse peak power	250 W
Pulse repetition rate	12.5 kHz
AOM frequency shift	80 MHz
AOM extinction ratio	80 dB
Transceiver:	
Telescope diameter	100 mm
Focal length	550 mm
Beam full divergence	44 μrad
Circulator isolation	30 dB
Receiver:	
Receiving bandwidth	220 MHz
Sample rate	500 MSps
Temporal resolution	1 s

and the modulating sequence. An erbium-doped fiber amplifier (EDFA, Amonics ALiDAR-150-AMP) is employed to amplify the coded pulses. Benefiting from the large core diameter of the EDFA's output fiber, the peak power can be amplified to 250 W without being distorted by the stimulated Brillouin scattering. After amplification, the phase coded pulses are transmitted to the atmosphere by a 100-mm telescope, which is also used to collect the atmospheric backscattered signal. Guided by a circulator, the received optical signal is mixed with the LO and down converted into electrical signal in IF band after beating on a balanced photodetector (BPD). The analog bandwidth of the receiver is limited to 220 MHz to avoid frequency aliasing when digitized by an analog-to-digital converter (ADC) at 500 MSps. The digitized raw data are stored in a computer for offline processing with the algorithm depicted in Fig. 4. The temporal resolution is set to 1 s, accumulating the backscattered spectra from 12.5k laser shots. The key system parameters are summarized in Table I.

B. Proof-of-Concept Experiment

In a first experiment, the performance of CDWLs based on PRPC method and conventional non-coding (NC) method is compared. The FWHM of the pulse intensity envelope in the PRPC lidar is 185 ns and the modulation bit interval is 100 ns. Meanwhile, the FWHM pulse duration of the NC lidar is

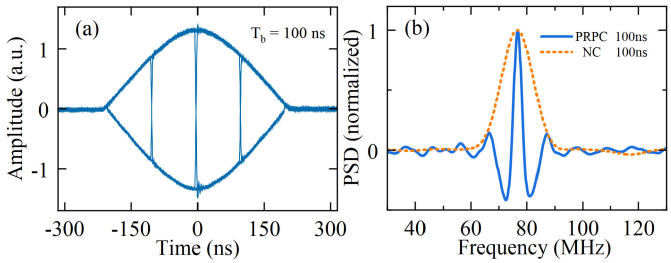

Fig. 6. (a) Eye diagram of the coded pulses with $T_b = 100$ ns. (b) Comparison of the normalized backscattered spectra obtained by the PRPC and NC methods.

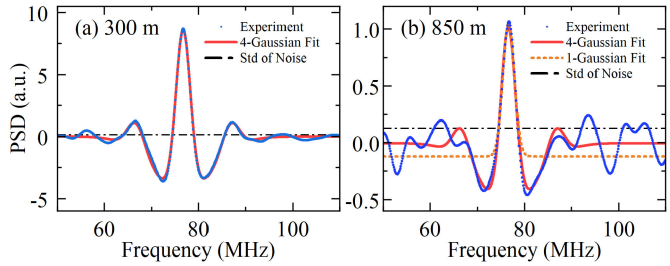

Fig. 7. Spectra measured by the PRPC-100ns lidar at (a) 300 m and (b) 850m and corresponding Gaussian fits.

set to be 100 ns to achieve similar spatial resolution. Other parameters of NC lidar are shared with PRPC lidar as in Table I. For brevity, the two systems will be referred to as PRPC-100ns and NC-100ns, according to the time parameter directly related to spatial resolution.

During the experiments, the modulated lightwave is first monitored by homodyne detection with a 180°optical hybrid [26]. Fig. 6(a) shows the eye diagram of the transmitted signal, which is formed by overlaying the coded pulses' electric field. The transition time between different bits is about 5 ns, limited by the AWG's analog bandwidth. After collecting the raw data in time domain, the range resolved PSD can be got by the periodogram [15]. A Gaussian window with FWHM of 270 ns is used to match the electric field envelope of the pulses. For each spectrum, the fast Fourier transform (FFT) length is extended to 4096 through zero padding with frequency sampling interval of 0.122 MHz. As an example, the backscattered spectra at 300 m are shown in Fig. 6(b). To display the difference of spectral width clearly, the spectra of the two methods are normalized by the peak value. Since the width of the main spectral peak in PRPC method is decided by the pulse envelope rather than modulation rate, the PRPC-100ns has a sharper spectrum compared with the NC-100ns, which is beneficial to the center frequency estimation accuracy [14].

The center frequency of the PRPC method can be estimated with the 4-Gaussian model described in Section II. When the carrier-to-noise ratio (CNR) is high, the spectrum measured in experiment can be well fitted by the model, as shown in Fig. 7(a). However, when the secondary peak with center shift R_b is seriously corrupted by noise, the center estimation would not benefit from the multi-peak structure. Then, 1-Gaussian fit should be used to focus on the main peak, as shown in Fig. 7(b).

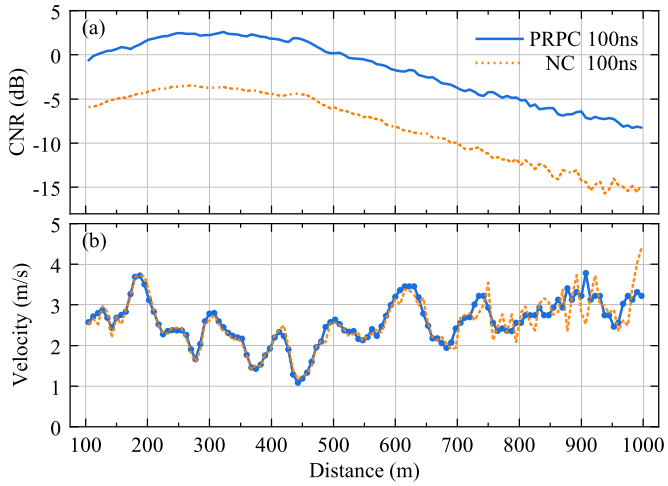

Fig. 8. (a) Narrowband CNR and (b) radial wind velocity profiles of the PRPC and the NC lidar.

A practical criterion is whether the fitted secondary peak exceeds the standard deviation (std) of the noise.

In a wind profiling experiment, measurement results of lidars with the two different configurations are plotted in Fig. 8, where the blue solid line and orange short-dash line stand for the PRPC-100ns and NC-100ns, respectively. Fig. 8(a) shows the narrowband CNR [27] of the two methods. In the PRPC method, the narrowband CNR is calculated by the power of the fitted main peak divided by the noise power under the peak. Compared with NC-100ns, the PRPC-100ns has higher CNR at the same spatial resolution and laser peak power. Admittedly, the NC-100ns has a smaller pulse energy due to its short pulse duration. But it should be recognized that this deterioration in pulse energy is inevitable. Since the spatial resolution and pulse duration in the NC method are coupled, to get specific spatial resolution under limited peak power, the pulse energy has to be confined.

The wind velocity is derived from the Doppler frequency shift estimated by the Gaussian fit. In this work, 1-Gaussian model is used for simplicity. In Fig. 8(b), the radial wind velocity profiles measured by the two methods are quite consistent within 600 m, confirming the PRPC lidar's spatial resolution. Between 600 and 1000 m, the profile of NC-100ns fluctuates around that of PRPC-100ns due to the low CNR.

C. High-Spatial-Resolution Wind Profiling

To further explore the performance of the PRPC method, a second experiment is carried out at a high spatial resolution of 4.5 m. According to (5), the modulation bit interval is 30 ns and the FWHM of the pulse intensity envelope is optimized to 135 ns. The FWHM of the Gaussian window function is set to be 160 ns. To validate the measurement by the PRPC lidar, a NC lidar with the same pulse intensity envelope is used as a reference. The spatial resolution of the NC lidar is about 20 m, estimated by the pulse duration. The instruments are placed on the 9th floor of the laboratory building with the telescope pointing horizontally.

The eye diagram of the transmitted pulses in PRPC-30 ns is shown in Fig. 9(a). After accumulation for 1 s, the normalized

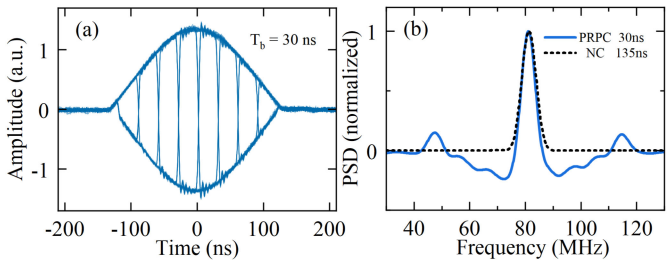

Fig. 9. (a) Eye diagram of the coded pulses with $T_b = 30$ ns. (b) Comparison of the normalized backscattered spectra obtained by the PRPC and NC methods.

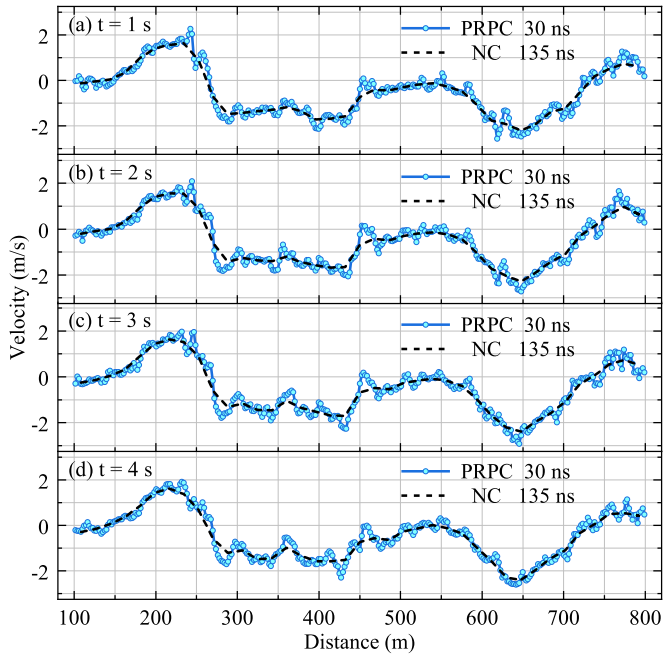

Fig. 10. Radial wind velocity profiles obtained by continuous observation over 4 s. (a)-(d) The PRPC and the NC lidar measurements with temporal resolution of 1 s.

backscattered spectra at 300 m are compared in Fig. 9(b). Since pulses with the same intensity envelope are employed, the spectral widths of PRPC-30ns and NC-135ns are quite close. Meanwhile, if narrowing the pulse duration in a NC lidar to achieve the same spatial resolution as the PRPC-30ns, the backscattered spectrum will be greatly broadened, making it hard to retrieve the Doppler frequency shift [28].

Fig. 10 shows the wind velocity profiles obtained by the two methods, where the blue marked line and black dash line stand for the PRPC-30 ns and NC-135 ns, respectively. Continuous profiling over 4 s is conducted to observe the evolution of atmospheric wind field. As illustrated in Fig. 10, the two sets of lines have the same trend versus distance. Differences between the two lidars' measurements are observed at some distances (like 450 m), which can be attributed to the low spatial resolution of the NC-135 ns. Influenced by the buildings on the campus, there could be some fine structures in the wind field. Under a lower spatial resolution, the wind profiles of the NC-135 ns are smoothed, showing less details compared

with the PRPC-30 ns. During the experiment, the profile of the PRPC-30 ns changes continuously around that of the NC-135 ns. This continuity conforms the time-varying characteristics of the wind field, which further verifies the reliability of the measurement.

IV. Discussion

In conventional pulsed CDWLs, both the spectrum width and the spatial resolution are related to the pulse duration. The PRPC method decouples two of the three parameters, making the pulse duration configurable under a certain spatial resolution. This flexibility allows more energy to be contained in one pulse under limited peak power, thereby improving the narrowband CNR [27]. Even at the same pulse energy, a narrow spectrum can still benefit the center frequency estimation [14]. However, as illustrated in Fig. 2, increasing the pulse duration will also reduce the energy proportion of the despread spectrum, making it more vulnerable to the interference of the spread spectrum and noise. In addition, the specular reflection from the output optics in a monostatic configuration will increase the blind area [29], which is unfavorable in some applications. Trade-offs need to be made based on requirements. Indeed, optimizing the pulse duration and modulation scheme for specific applications is a comprehensive work to be done.

The spatial resolution of the proposed system can be further upgraded by increasing the modulation rate. It is worth noting that although the Doppler frequency shift is estimated by the narrow main peak after decoding, a wide bandwidth is still required by the receiver. Since the decoding is conducted in time domain, if the undecoded signal is distorted by the limited bandwidth, the results could be contaminated by the inter symbol interference (ISI) [30]. Hence, to further improve the spatial resolution, the bandwidth of both the transmitter and the receiver needs to be increased to support encoding and decoding at higher rate.

In our previous work [18], the DCP technique is used to enhance the spatial resolution of CDWLs by the amplitude modulation of paired pulses and corresponding data processing algorithm. Due to the time-dependent gain profile of the EDFA [29], the modulating signals need to be particularly designed to minimize the difference between the amplified common parts in one pulse pair. And the environmental disturbance may be introduced into the system through the EDFA's gain profile. In this work, the proposed PRPC method is insensitive to the intensity fluctuation, making it more robust. Moreover, since the measurement of the PRPC lidar relies on the spectra accumulation of each pulse rather than pair, nearly half of the average power can be saved compared to the DCP method at the same resolution.

Considering that the phase modulation doesn't change the intensity envelope of pulses, the PRPC method can be migrated to the conventional pulsed CDWLs with only minor changes in hardware (i.e., inserting a EOPM and its driver). This compatibility allows it to be used to upgrade existing systems and significantly accelerates the development and application of the new method.

V. Conclusion

A CDWL with meter-scale spatial resolution incorporating PRPC technique is proposed and experimentally demonstrated. The new method offers an approach to improve the spatial resolution without broadening the spectrum peak. Benefiting from the spectrum spreading effect of the pseudo-random code, the backscattered signals from different distances can be separated in the decoding process and extracted by a difference operation. The performance of the proposed system is validated in experiments. By comparing with non-coding CDWLs, the spatial resolution and spectrum feature of the PRPC lidar are confirmed. The system has the potential of applying to areas such as aviation safety and aerodynamic research where high spatial resolution wind profiles are required. In addition, due to its compatibility with conventional non-coding scheme, the proposed method has the opportunity to enhance the spatial resolution of deployed CDWLs.

References

[1] B. Witschas, S. Rahm, A. Dörnbrack, J. Wagner, and M. Rapp, "Airborne wind lidar measurements of vertical and horizontal winds for the investigation of orographically induced gravity waves," *J. Atmos. Ocean. Technol.*, vol. 34, no. 6, pp. 1371–1386, Jun. 2017.

[2] M. Jia *et al.*, "Long-lived high-frequency gravity waves in the atmospheric boundary layer: Observations and simulations," *Atmos. Chem. Phys.*, vol. 19, no. 24, pp. 15431–15446, Dec. 2019.

[3] Y. Yang *et al.*, "Diurnal evolution of the wintertime boundary layer in urban beijing, China: Insights from doppler lidar and a 325-m meteorological tower," *Remote Sens.*, vol. 12, no. 23, Dec. 2020, Art. no. 3935.

[4] T. Mikkelsen, "Lidar-based research and innovation at DTU wind Energy–a review," *J. Phys. Conf. Ser.*, vol. 524, Jun. 2014, Art. no. 012007.

[5] N. J. Harvey, R. J. Hogan, and H. F. Dacre, "Evaluation of boundary-layer type in a weather forecast model utilizing long-term doppler lidar observations," *Q. J. R. Meteorol. Soc.*, vol. 141, no. 689, pp. 1345–1353, Apr. 2015.

[6] Y. Yang *et al.*, "Characteristics of heavy particulate matter pollution events over Hong Kong and their relationships with vertical wind profiles using high-time-resolution doppler lidar measurements," *J. Geophys. Res.: Atmos.*, vol. 124, no. 16, pp. 9609–9623, Dec. 2019.

[7] T. Huang *et al.*, "Assessing transboundary-local aerosols interaction over complex terrain using a doppler LiDAR network," *Geophys. Res. Lett.*, vol. 48, no. 12, Jun. 2021, Art. no. 2021GL093238.

[8] T. Wei, H. Xia, B. Yue, Y. Wu, and Q. Liu, "Remote sensing of raindrop size distribution using the coherent doppler lidar," *Opt. Exp.*, vol. 29, no. 11, pp. 17246–17257, May 2021.

[9] J. Yuan *et al.*, "Cloud seeding evidenced by coherent doppler wind lidar," *Remote Sens.*, vol. 13, no. 19, Sep. 2021, Art. no. 3815.

[10] J. Yuan, H. Xia, T. Wei, L. Wang, B. Yue, and Y. Wu, "Identifying cloud, precipitation, windshear, and turbulence by deep analysis of the power spectrum of coherent doppler wind lidar," *Opt. Exp.*, vol. 28, no. 25, pp. 37406–37418, Dec. 2020.

[11] I. N. Smalikho and V. A. Banakh, "Estimation of aircraft wake vortex parameters from data measured with a 1.5 um coherent doppler lidar," *Opt. Lett.*, vol. 40, no. 14, pp. 3408–3411, Jul. 2015.

[12] I. N. Smalikho, V. A. Banakh, F. Holzäpfel, and S. Rahm, "Method of radial velocities for the estimation of aircraft wake vortex parameters from data measured by coherent doppler lidar," *Opt. Exp.*, vol. 23, no. 19, pp. A1194–A1207, Sep. 2015.

[13] S. Wu, X. Zhai, and B. Liu, "Aircraft wake vortex and turbulence measurement under near-ground effect using coherent doppler lidar," *Opt. Exp.*, vol. 27, no. 2, pp. 1142–1163, Jan. 2019.

[14] B. J. Rye and R. M. Hardesty, "Discrete spectral peak estimation in incoherent backscatter heterodyne lidar. I. Spectral accumulation and the cramer-rao lower bound," *IEEE Trans. Geosci. Remote Sens. Lett.*, vol. 31, no. 1, pp. 16–27, Jan. 1993.

[15] R. G. Frehlich and M. J. Yadlowsky, "Performance of mean-frequency estimators for doppler radar and lidar," *J. Atmos. Ocean. Technol.*, vol. 11, no. 5, pp. 1217–1230, Oct. 1994.

[16] N. Prasad, R. Sibell, S. Vetorino, R. Higgins, and A. Tracy, "An all-fiber, modular, compact wind lidar for wind sensing and wake vortex applications," *SPIE Defense+Secur.*, 2015, vol. 9465, pp. 101–111, doi: 10.117/12.2181170.
[17] C. Wang, H. Xia, Y. Wu, J. Dong, and X. Dou, "Meter-scale spatial-resolution-coherent doppler wind lidar based on golay coding," *Opt. Lett.*, vol. 44, no. 2, Jan. 2019, Art. no. 311.
[18] Y. Zhang, Y. Wu, and H. Xia, "Spatial resolution enhancement of coherent doppler wind lidar using differential correlation pair technique," *Opt. Lett.*, vol. 46, no. 22, pp. 5550–5553, Nov. 2021.
[19] M. A. Richards, *Fundamentals of Radar Signal Processing*, New York, NY, USA: McGraw-Hill Education, 2014.
[20] I. Toru, Y. Yoshikawa, S. Izumi, and H. Kawaguchi, "Subcentimeter precision ranging system for moving targets with a doppler-effect- compensated ultrasonic direct sequence spread spectrum," *IEEE Trans. Instrum. Meas.*, vol. 70, Dec. 2021, Art. no. 9505008.
[21] Z. Xu, F. Yu, B. Qiu, Y. Zhang, Y. Xiang, and S. Pan, "Coherent random-modulated continuous-wave LiDAR based on phase-coded subcarrier modulation," *Photonics*, vol. 8, no. 11, Oct. 2021, Art. no. 475.
[22] S. Banzhaf and C. Waldschmidt, "Phase-Code-Based modulation for coherent lidar," *IEEE Trans. Veh. Technol.*, vol. 70, no. 10, pp. 9886–9897, Oct. 2021.
[23] F. Yang, Y. He, W. Chen, and Y. Zhan, "Laser altimeter based on random code phase modulation and heterodyne detection," *IEEE Photon. Technol. Lett.*, vol. 26, no. 23, pp. 2337–2340, Dec. 2014.
[24] J. G. Proakis and M. Salehi, "Spread spectrum signals for digital communications," in *Digital Communications*, 5th ed. New York, NY, USA: McGraw-Hill Education, 2007, ch. 12.
[25] P. Salamitou, A. Dabas, and P. H. Flamant, "Simulation in the time domain for heterodyne coherent laser radar," *Appl. Opt.*, vol. 34, no. 3, pp. 499–506, Jan. 1995.
[26] K. Kikuchi, "Fundamentals of coherent optical fiber communications," *J. Lightw. Technol.*, vol. 34, no. 1, pp. 157–179, Jan. 2016.
[27] S. W. Henderson, P. Gatt, D. Rees, and R. M. Huffaker, "Wind lidar," in *Laser Remote Sensing*, T. Fujii and T. Fukuchi Eds., Boca Raton, FL, USA: CRC, 2005, ch. 7, pp. 33487–32742.
[28] C. Wang, H. Xia, Y. Liu, S. Lin, and X. Dou, "Spatial resolution enhancement of coherent doppler wind lidar using joint time–frequency analysis," *Opt. Commun.*, vol. 424, pp. 48–53, Jan. 2018.
[29] P. Schroeder, W. A. Brewer, A. Choukulkar, A. Weickmann, and S. Sandberg, "A compact, flexible, and robust micropulsed doppler lidar," *J. Atmos. Ocean. Technol.*, vol. 37, no. 8, pp. 1387–1402, Aug. 2020.
[30] J. G. Proakis and M. Salehi, "Digital communication through band-limited channels," in *Digital Communications*, 5th ed., New York, NY, USA: McGraw-Hill Education, 2007, ch. 9, Art. no. 10020.